Transverse Oscillations of Coronal Loops induced by eruptions of Magnetic Flux Tube and Plasmoid

Safna Banu K.
National Institute of Technology Calicut
R. A. Maurya (ramajor@nitc.ac.in)
National Institute of Technology Calicut
Jain Jacob P.T.
National Institute of Technology Calicut

Research Article

Keywords: Corona, Structures, Flares, Pre-Flare Phenomena, Flares, Waves; Waves, Magnetohydrodynamic, Waves, Shock

Posted Date: May 16th, 2022

DOI: https://doi.org/10.21203/rs.3.rs-1633181/v1

Transverse Oscillations of Coronal Loops induced by eruptions of Magnetic Flux Tube and Plasmoid

Safna Banu K.[1] · **R. A. Maurya**[1] · **Jain Jacob P. T.**[1]

Abstract

We studied the transverse oscillations in hot coronal loops of an active region NOAA 12673 located at the west limb. Loop oscillations were associated with a plasmoid ejection from the same area. During the rising phase of the plasmoid, a magnetic flux tube was seen to be rising and bending towards the loop system that erupted before the plasmoid ejection. In addition to the plasmoid ejection, a large coronal mass ejection (CME) and a X8.2 flare was observed in the same active region for several hours ($\sim$ 7 hours). A follow-up shock wave from the flare site after the plasmoid ejection was possibly triggered by sudden momentum transfer towards the solar disc. It was found to be propagating across the entire solar disc with an average speed of $\sim$ 1290 km s^{-1}. The combined effects of the erupting flux tube, plasmoid ejection and the shock wave perturbed the loops from their equilibrium and set them in oscillations. We found different oscillations of fundamental mode in loops, fast decaying (with a period of 7.20 minutes and a damping time of $\sim$ 16.00 minutes) and slow decaying (with a period of $\sim$ 5.75 minutes and a damping time of $\sim$ 30.78 minutes). The two different oscillations could be due to different loop lengths and plasma densities. These loops were found to be oscillating with a phase difference of $\sim$ 33 degrees. This could be due to varying times of their excitation, possibly caused by the flux tube's eruption and the plasmoid ejection.

Keywords: Corona, Structures; Flares, Pre-Flare Phenomena; Flares, Waves; Waves, Magnetohydrodynamic; Waves, Shock

1. Introduction

Coronal loops are closed magnetic structures in the form of loops embedded into the coronal plasma. They are rooted in the interior below the photosphere and are affected by the dynamics of the interior plasma and the activities in the atmosphere. However, it is still a mystery what drives them to be vertically standing against the strong solar gravity. They are found to be swaying during energetic activities such as flares, Coronal Mass Ejections (CMEs), etc.

Solar flares are the results of the magnetic reconnection—tangling, crossing and reorganization of magnetic field lines (Shibata, 1996) in which the magnetic energy is transformed to the kinetic energy of rapidly moving CMEs, particle acceleration and thermal energy to heat the plasma (Yokoyama *et al.*, 2001). A pre-flare can also trigger a large flare on a

✉ R.A. Maurya
ramajor@nitc.ac.in

Safna Banu K.
safna˙p180029ph@nitc.ac.in

Jain Jacob P. T.
jain˙p180130ph@nitc.ac.in

[1] Department of Physics, National Institute of Technology Calicut, Kerala-673601

stable flux tube which destabilize the ropes (Nindos *et al.*, 2015; Mitra and Joshi, 2019) and can initiate waves and oscillations in coronal loops. Standing kink mode oscillations may be produced through interactions of contracting loops with underlying loops (Russell, Simões, and Fletcher, 2015), ejection of jets or plasmoids from the flaring site (Zimovets and Nakariakov, 2015), and eruption of filament or flux rope. They can also generate a shock waves by sudden deposition of the energy at flare site. However, the excitation mechanism of the coronal loop oscillations is still debatable.

Flare induced transverse coronal loop oscillations were initially reported by Aschwanden *et al.* (1999) using observations provided by the Transition Region and Coronal Explorer (TRACE), and later on using the observations provided by the Atmospheric Imaging Assembly (AIA) onboard Solar Dynamic Observatory (SDO) (Aschwanden and Schrijver, 2011), and by some other researchers (Nakariakov *et al.*, 2021). They found the period of oscillations to be around 6.3 minutes with a quality factor $\gg 4$, in vertically polarized mode. The oscillation period is proportional to the length of the loops with exponential damping (Goddard *et al.*, 2016). These oscillations attenuate gradually after a few periods of oscillation due to different damping processes such as dissipative damping (Nakariakov *et al.*, 1999), phase mixing (Heyvaerts and Priest, 1983), resonant absorption (Hollweg and Yang, 1988), cooling of plasma (White and Verwichte, 2012; White, Verwichte, and Foullon, 2013) and mode coupling (Pascoe *et al.*, 2012). However, the damping mechanism of the loop oscillations is not yet fully understood.

Most of reported coronal loop oscillations are fast asymmetric kink oscillations (Nakariakov and Verwichte, 2005). The kink mode oscillations are classified into two types: high amplitude with decaying oscillations and low amplitude with decay-less oscillations (Nakariakov *et al.*, 1999; Anfinogentov, Nisticò, and Nakariakov, 2013; Nisticò, Nakariakov, and Verwichte, 2013). These oscillations are generally periodic displacements of coronal loops and are in the fundamental mode of oscillations (Nakariakov *et al.*, 1999; Jain, Maurya, and Hindman, 2015). In some events, the harmonics are also reported (Moortel and Brady, 2007; Doorsselaere, Nakariakov, and Verwichte, 2007; White and Verwichte, 2012). These oscillations can be used to study the physical properties of the coronal plasma.

The information of coronal magnetic field is essential as it provides understanding of solar activities in its atmosphere. But we have not yet succeed in the direct measurement of coronal magnetic field with available methodology. Coronal waves and oscillations provide us an indirect method to diagnose the plasma properties similar to the helioseismology for the solar interior. They can be used to estimate the physical parameters of the solar corona, such as internal Alfvén speed, magnetic field strength and density structures of coronal loops. For more details about the recent reports on the observations and theoretical modelling of coronal oscillations, the reader may refer to a recent review article by Nakariakov *et al.* (2021).

This paper analyses the properties of transverse coronal loops excited by a rising flux tube and plasmoid ejections. We estimated the kink speed and the magnetic field in the coronal loops. Section 2 provides a detailed description of the observational data used. The analysis and results are presented in Section 3. Finally, the summary and discussions are given in Section 4.

2. Observational Data

For this study, we used the observations provided by the SDO/AIA, specifically, the extreme ultraviolet (EUV) 171 Å intensity images of 10 September 2017 during 15:00 UT to 17:00 UT. The EUV 171Å intensity images show emissions mainly in Fe IX from the solar plasma at the upper transition region and quiet corona at temperature, $T = 0.63$ MK (O'Dwyer *et al.*, 2010; Lemen *et al.*, 2011). These observations are taken with a pixel resolution of $0''.6$ and a temporal resolution of 12 s. To study the flare energetics in X-rays, we have also utilized the observations provided by the Geosynchronous Operational Environmental Satellites (GOES) in the $0.5 - 4$Å and $1 - 8$Å wavelength bands. Flare associated CME is analyzed using the data obtained from the C2 and C3 coronagraphs of the Large Angle and Spectrometric Coronograph (LASCO) (Brueckner *et al.*, 1995) onboard the Solar and Heliospheric Observatory (SOHO).

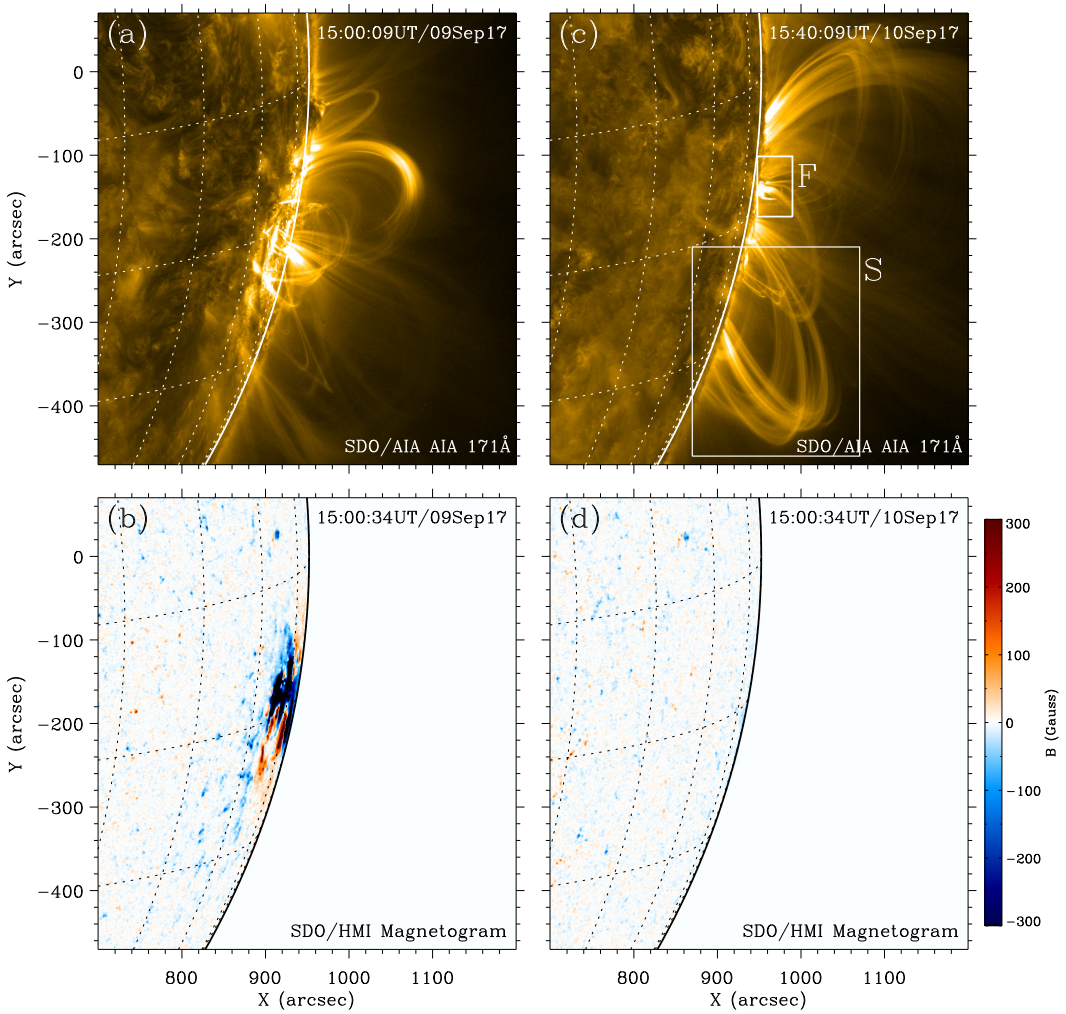

Figure 1. A sample of the SDO/AIA 171Å intensity images (top row) and the SDO/HMI magnetograms (bottom row) covering the active region NOAA 12673 and associated coronal loops. In panel (c), the small box 'F' marks the flare site, and the box 'S' represents the coronal loops that are considered for the oscillation studies.

3. Analysis and Results

The results of our analysis are shown in Figures 1 - 11.

3.1. The Active Region and the Oscillating Coronal Loops

The active region NOAA 12673 emerged in the far-side of the solar disc, and it was first observed as a simple sunspot region at the west limb around at a south latitude of 8 degree on 28 August 2017. It evolved to a complex active region on 9-10 September 2017 while crossing the disc near the west limb (see Figure 1). It has produced several energetic flares, such as 38 C-class, 20 M-class and 2 X-class, during crossing the disc from the east to west limb. The line-of-sight magnetic fields in the active region on and before the day of the initiation of an X8.2 flare (10 September 2017) are shown in Figure 1 (bottom panel). On 10 September, in the magnetogram (panel d), most of the active region area is on the far-side of the solar disc, which forbade us to analyze the activity related changes in the magnetic fields at the photosphere. However, the coronal loops associated with the active region can be seen in the AIA's EUV observations, such as 171 Å intensity images (panel c), because of their heights above the photosphere.

The oscillating coronal loops (marked by the box 'S') are located southward from the flare site (labeled by 'F'). These coronal loops were almost visible in all AIA passband such as 171 Å, 211 Å, 193 Å and 131 Å, weakly in 335 Å and 94 Å(see Figure 2), which indicates

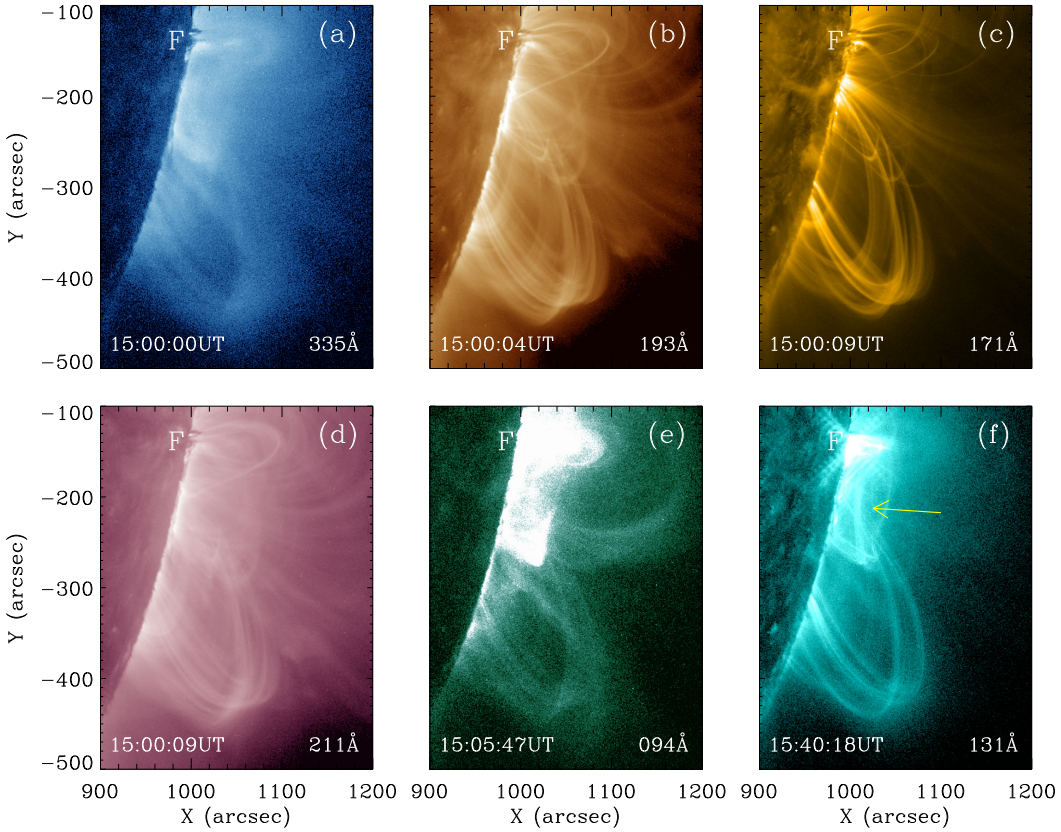

Figure 2. Observations of coronal loops in different SDO/AIA channels.

that the loops have a temperature distribution of 0.3 to 2 MK and most of them are warm loops. They seem to be inclined towards the south from the vertical. A careful analysis of magentograms taken a few days before the flare and EUV images showed that footpoints of these loops are rooted in the same active region. This region have a mixed magnetic polarities. A dominant-negative(positive) polarity region is found to be located northern (southern) side of the active region center. There are diffused magnetic fields with opposite polarities in the nearby regions. There are no other active regions in its neighbouring areas. The coronal loops marked by the box 'S' are the part of this active region. One of the foot points of these loops are located near the centre of the active region and the other in the diffused magnetic polarity regions in the southern areas. The X8.2 flare is seen in the region marked by 'F', and a plasmoid ejection is found to be rising vertically from it.

3.2. Pre-flare, Plasmoid Ejections and the onset of the Loop Oscillations

Figure 3 shows the normalized flare intensity profile in the AIA EUV 171Å from the flare site 'F' (marked by a small box in the Figure 1c) and the normalized integrated GOES soft X-ray fluxes in the wavelength bands $0.5 - 4.0$ Å. The AIA intensity curve shows two peaks, one at 15:45:33 UT and the other at 16:07:21 UT. The first peak corresponds to a small flare (say pre-flare) and the second corresponds to a large flare X8.2 (say main flare). In the AIA 171 Å, the pref-flare started at 15:39 UT and ended at 15:50 UT. But the pre-flare emissions are not observed in the GOES X-ray flux profile. The main flare intensity enhances in the AIA 171 Å just after the pre-flare while in GOES X-ray it started at 15:45 UT, *i.e.*, during the pre-flare seen in the AIA 171Å. The main flare peak time in GOES occurs at 16:03:17 UT, *i.e.*, ∼5 minutes before the peak timing of the flare in AIA 171Å. The main flare intensity in AIA 171Å ended nearly at 23:00 UT, *i.e.*, it lasted for several hours (∼ 7 hours), while it decayed much faster in GOES X-rays. The long decay phase in AIA 171 Å emissions is caused by heating of the coronal loops at higher altitudes above the flare site (see Figure 4i).

For a detailed analysis of activities associated changes in the magnetic field configurations, we have plotted a sample of AIA 171Å intensity images in the Figure 4. This shows rising

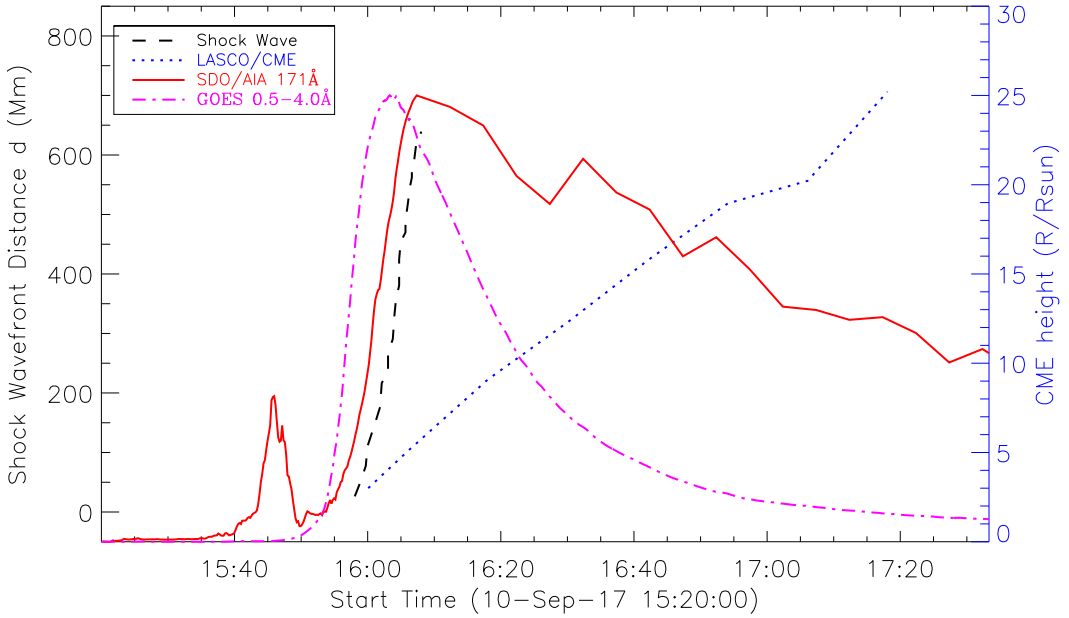

Figure 3. Relationship between flare induced shocks and associated CME. The dashed black curve shows the shock wave front position along the slit '6' direction (see Figure 7(a)). The dotted blue curve marks the CME's height from the solar surface. The normalized profiles of SDO/AIA 171Å intensity (solid red curve) and GOES X-ray flux (dashed-dotted magenta) are plotted for reference.

of a plasmoid, bending of flux tubes and occurrence of the main flare. In AIA 131Å (see Figure 2f), we observed that a magnetic flux rope starts rising at 15:40:18 UT and undergoes an impulsive acceleration phase around at 15:46:56 UT. But in the AIA 171Å intensity images, we observed magnetic flux rope (MFR) associated with the pre-flare that rises at 15:49:45 UT with a filament. It grew rapidly and triggered a fast eruption. That is, we only observed the acceleration phase of the MFR in the AIA 171Å intensity images. During the pre-flare time, a small loop labeled with number '2' whose one of the footpoints is in the flare site starts to expand southward at 15:41:21 UT.

At the flare site 'F', we also found a small C1-class flare at 15:23:21 UT that triggered a small oscillations in the coronal loop marked by number '5' (Figure 4a) at 15:31:45 UT. This loop detached from the footpoint at 15:37:45 UT and disappeared from the flare site at 15:39:33 UT. There after the pre-flare brightening was observed. It seems that the pre-flare triggered magnetic re-connections in other field lines that leads to the main flare at 15:52:09 UT.

To understand the relation between the flare and the oscillations of coronal loops, we have computed the space-time intensity maps along the reference lines AB and QP (see Figure 4b) and are shown in the Figure 5. Top panel shows the energetic activities such as flare, plasmoid ejection, etc. The bottom panel shows the perturbation in loops that triggered the transverse oscillations. During the pre-flare's end phase the plasma at higher altitude seems to be heated by the flare energy. This may also be due to re-connection of the field lines at higher atmosphere that resulted into the initiation of main flare. The pre-flare brightening at higher altitude disappeared around at 15:52 UT and the upward motion of a plasmoid was observed. That ejected around at 15:56 UT and pushed the field lines downward. We can also clearly see some flux tubes's rising during the plasmoid ejection. From the Figure 5, it is evident that the bending of the coronal loops happened during the rising time of the plasmoid from a nearby northern region.

In the equilibrium position of the loop, the inward magnetic tension force is balanced by the outward magnetic pressure gradient. When reorganization of magnetic field lines happen, it can release magnetic energy to the nearby places. This causes a reduction in the magnetic pressure in that area. Here, the rapid plasmoid ejection starts to form at 15:49:45 UT and resulted momentum transfer to the place where coronal loop '2' is located. Then the restoring magnetic tension comes to an action to balance the change in magnetic pressure and the loop have to move accordingly. We observed it as the bending of the loop '2' that suppressed

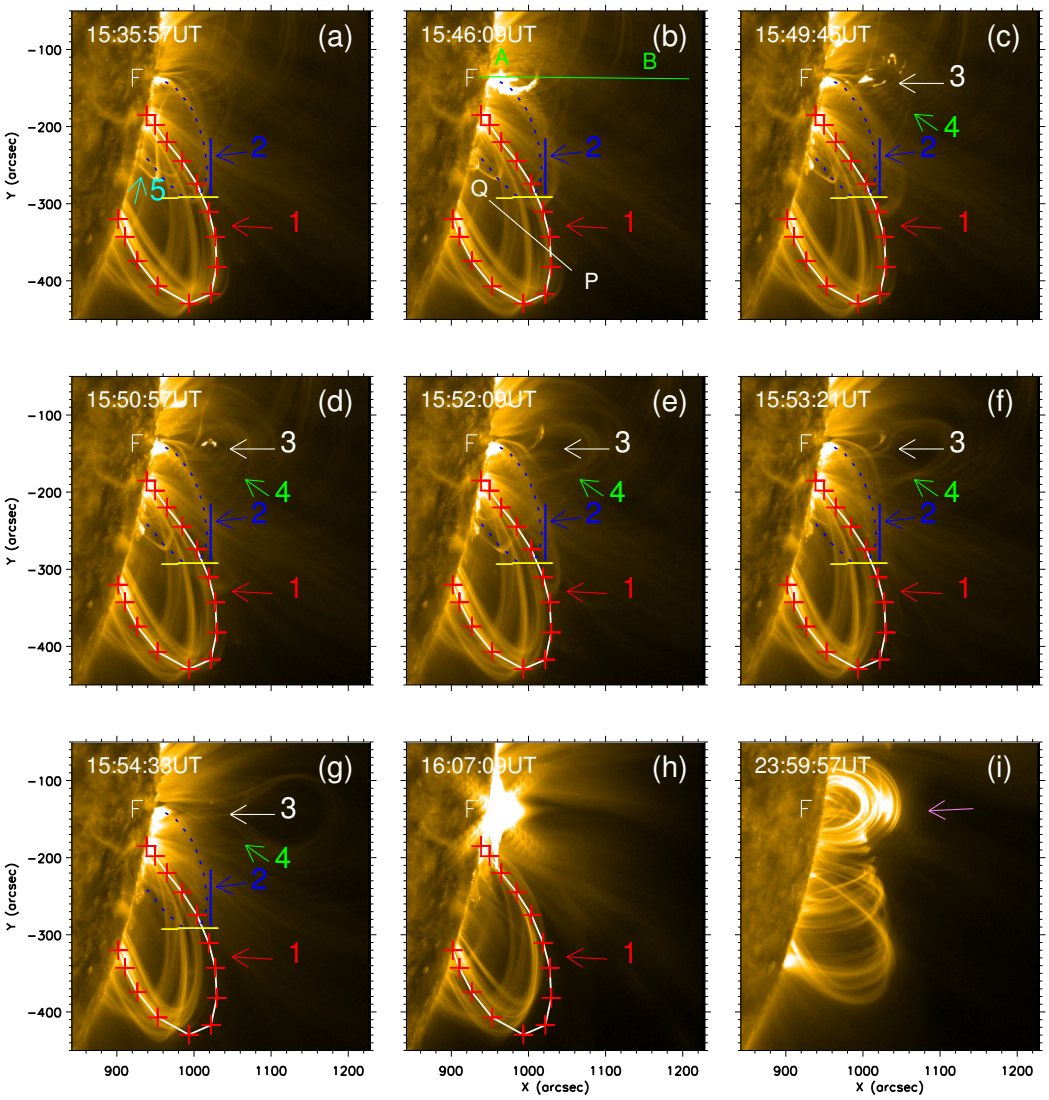

Figure 4. Image mosaic of the SDO/AIA 171Å intensity of the solar atmosphere covering the active region coronal loops. The flare position is marked by the letter 'F'. The white solid curve with red crosses labeled with number '1' represents a coronal loop that is used for the oscillation studies. The green line AB in the panel (b) illustrates the reference line along which a space time-map, associated with the plasmoid ejection (marked by the arrow 3), is computed and shown in the Figure (5a). Similarly, the solid line QP represents the reference position for analysing the transverse oscillations of coronal loop (see Figure 5b). The blue dotted curve in the panels, (a) - (g), represents the position of the coronal loop concerning the reference position marked by the horizontal (yellow) and the vertical (blue) lines. The violet arrow in panel (i) shows a system of post flare loops and their brightening at higher altitudes during the decay phase of the main flare.

the loop '1' to down till 16:25:09 UT (see Figure 4 c – g). Hence, the oscillations of large loops were initiated by the energy transported during the plasmoid formation and ejection from the flare site (Figure 5).

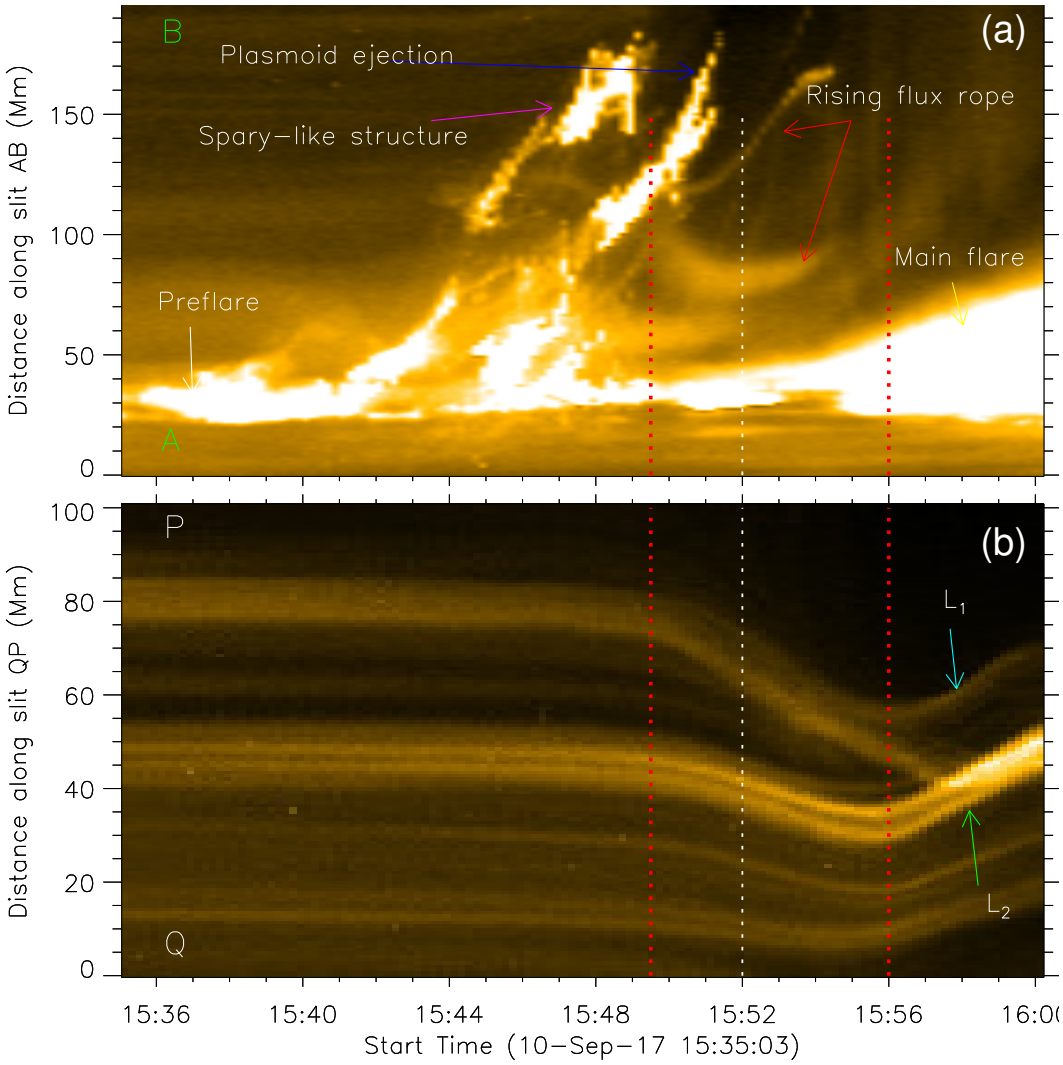

Figure 5. Association of the plasmoid ejection and the onset of loop oscillations. (a) Space-time map of the SDO/AIA 171Å intensity along the slit AB (see Figure 4b). (b) Similar to the panel (a) but along the slit QP (see Figure 4b). The vertical lines mark the timing of the plasmoid's start, the main flare's start and the maximum perturbation of coronal loops (from the left to the right).

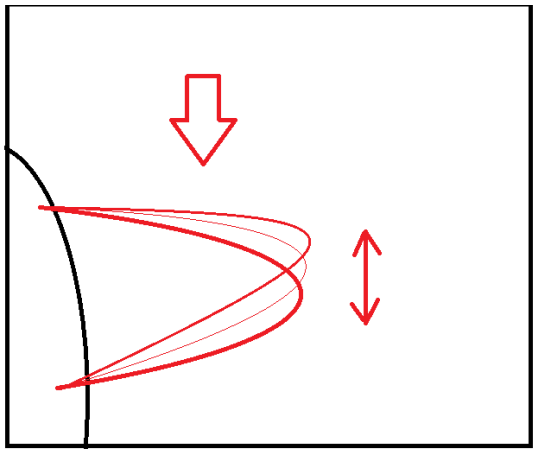

Figure 6. Transverse oscillations of the coronal loop '1' (see Figure 4), where red up and down arrows represent the oscillating direction. The red arrow pointing towards down shows that the perturbation comes from the top of the loop.

Figure 6 is used to illustrate the oscillations in the coronal loops. We think that the magnetic pressure force increased in loop '1' due to the suppression from top of the loop which is marked with red arrow. Then the restoring magnetic tension came to an action to reduce the excess pressure force by moving the loop '1' to upward and initiated oscillations in the loops. The loops are in kink oscillations but they appear to be moving radially up-down due to projection effects.

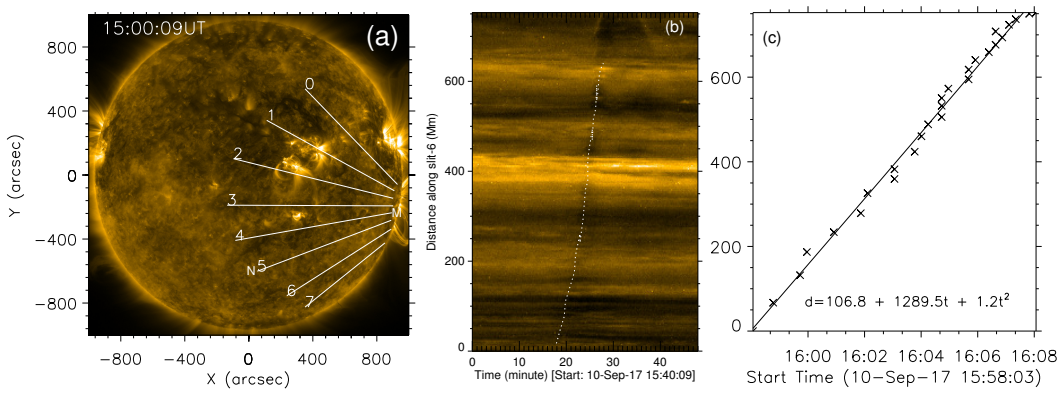

Figure 7. (a) Full disc AIA 171 Å intensity map, where white solid lines mark the slit positions for shock wave analysis. (b) The space-time intensity map along the slit-6, where the overlying white dashed curve represent the shock front position. (c) Least square quadratic fits the shock front position as shown in the panel (b).

3.3. Shock Waves and Coronal Mass Ejections

We observed a shock wave propagating away from the flare site. They propagated mostly towards the southward and part of it reflecting towards the north. To study the shock waves propagation across the disc and their role in the triggering of loop oscillations, we considered 8 slits along the direction of their propagation from the point of their initiation, see Figure 7(a). Further, to illustrated the wave propagation, we constructed a space-time intensity map along the slit-6 as the wave is seen in the bottom part of the solar disc. Thus the computed shock wave map is shown in the middle panel (b) of the Figure 7. The overlying white dashed curve marks the wavefront position. The shock wave starts around at 15:58 UT along slit-6 direction. We calculate the shock wave propagating speed along the slit-6 from the space-time map with a quadratic fits to the wavefront positions as shown in the right panel (c). We found the speed of the shock wave $\sim 1290\,\mathrm{km\,s^{-1}}$ with acceleration of $\sim 1.2\,\mathrm{km\,s^{-2}}$.

The shock wave first seen nearly at 15:54:00 UT in the impulsive phase of the flare and increases its velocity during the propagation. However, they might have started earlier as the flare site is hidden at the west limb. Hence, from the Figure 5, it seems that shock wave suppressed the coronal loops southward from the equilibrium and initiated oscillations.

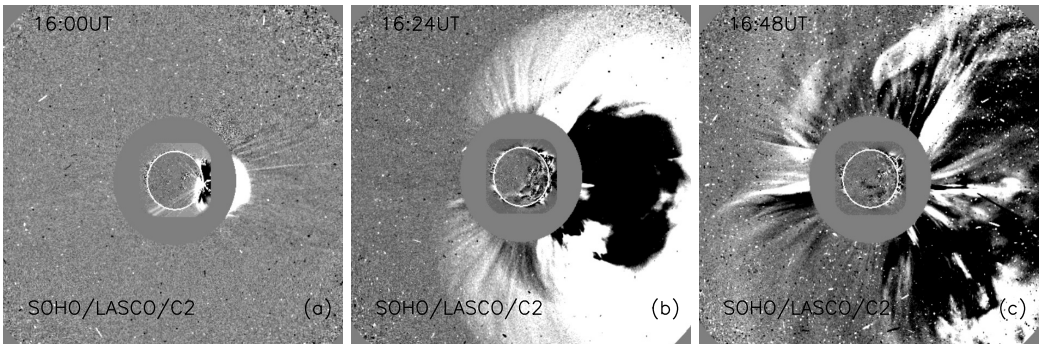

Figure 8. Intensity images of the Sun observed by SDO/AIA and SOHO/LASCO/C2 during start (a), peak (b) and propagation (c) times of the CME associated with the X8.2.

The SOHO/LASCO observations showed an halo CME associated with the main flare (see Figure 8), which first appeared around at 16:00 UT in C2 field of view (panel (a)), having a position angle of 263 degree and angular width of 360 degree. This CME is found to be moving with a speed of 3163 km s^{-1} and an acceleration of 232.0 ms^{-2} (see Figure 3). Gopalswamy *et al.* (2018) found that this CME was one of the highest eruption in the SOHO era with ground level enhancement (GLE) and solar energetic particle (SEP) events.

The relationship between the flare, CME and the shock wave's occurrence are shown in the Figure 3. The CME first appeared nearly at 16:00 UT, *i.e.*, along with the shock wave and after a few minutes of the main flare's starts seen in AIA 171Å and GOES X-ray fluxes. The impulsive acceleration phase of the CME merged with the rising phase of the main flare. In its propagation phase, the CME speed increases.

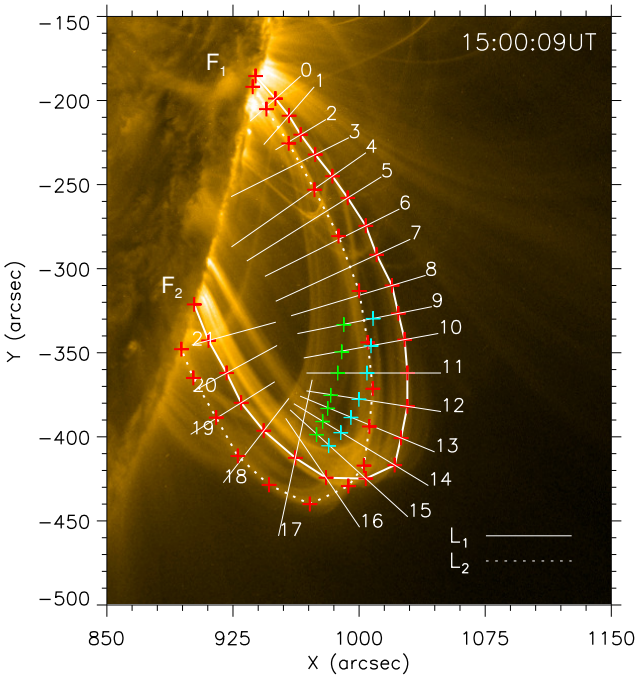

Figure 9: An SDO/AIA 171Å intensity image overlaid with marked coronal loops L_1 (solid curve) and L_2 (dashed curve) at 15:00:10 UT. F_1 and F_2 marked the footpoints of the coronal loops. The line segments 0 – 21 mark the slit positions perpendicular to the loop L_1 that are used to compute the space-time intensity maps as shown in the Figure 10. Cyan and green points represent the positions of loops L_1 and L_2, respectively at 15:56:10 UT

3.4. Transverse Oscillations of Coronal Loops

To analyse the properties of the transverse oscillations of coronal loops, we identified distinct loops in the AIA 171 Å intensity images and selected two oscillating loops named as L_1 and L_2 (see Figure 9) with sufficient quality for time-series analysis. Further to find the changes in the loop position as function of space and time, we took 22 slits across loops as shown in the Figure 9. Then space-time intensity maps for all slits were computed by combining the intensity values along different slits as a function of time. Thus the space-time intensity maps for 10 chosen positions are shown in the Figure 10. The amplitude of loop oscillations across all the slits and for all the loops decreases with time. We searched for a clear oscillatory patterns in coronal loops by analysing the space-time maps where at least three to four cycles of loop oscillations were seen. Thus we considered two loops marked by L_1 and L_2 as shown in the space-time map for the slit number 10. The time-series of the loop displacements were extracted from the space-time maps by following the loop intensity as a function of time. Thus the loop positions as a function of time are plotted in the top panel of the Figure 11 for the loop L_1 (left) and L_2 (right). Further to find the oscillations properties in the loops, we subtracted a linear trend for L_1 and a quadratic trend for L_2 from the time series, and the final time series is shown in the middle panels of the Figure 11. We determined the oscillation parameters by fitting an exponential damping cosine function of the form,

$$d(t) = A\cos\left(\frac{2\pi t}{P} + \phi\right) e^{-t/\tau}, \tag{1}$$

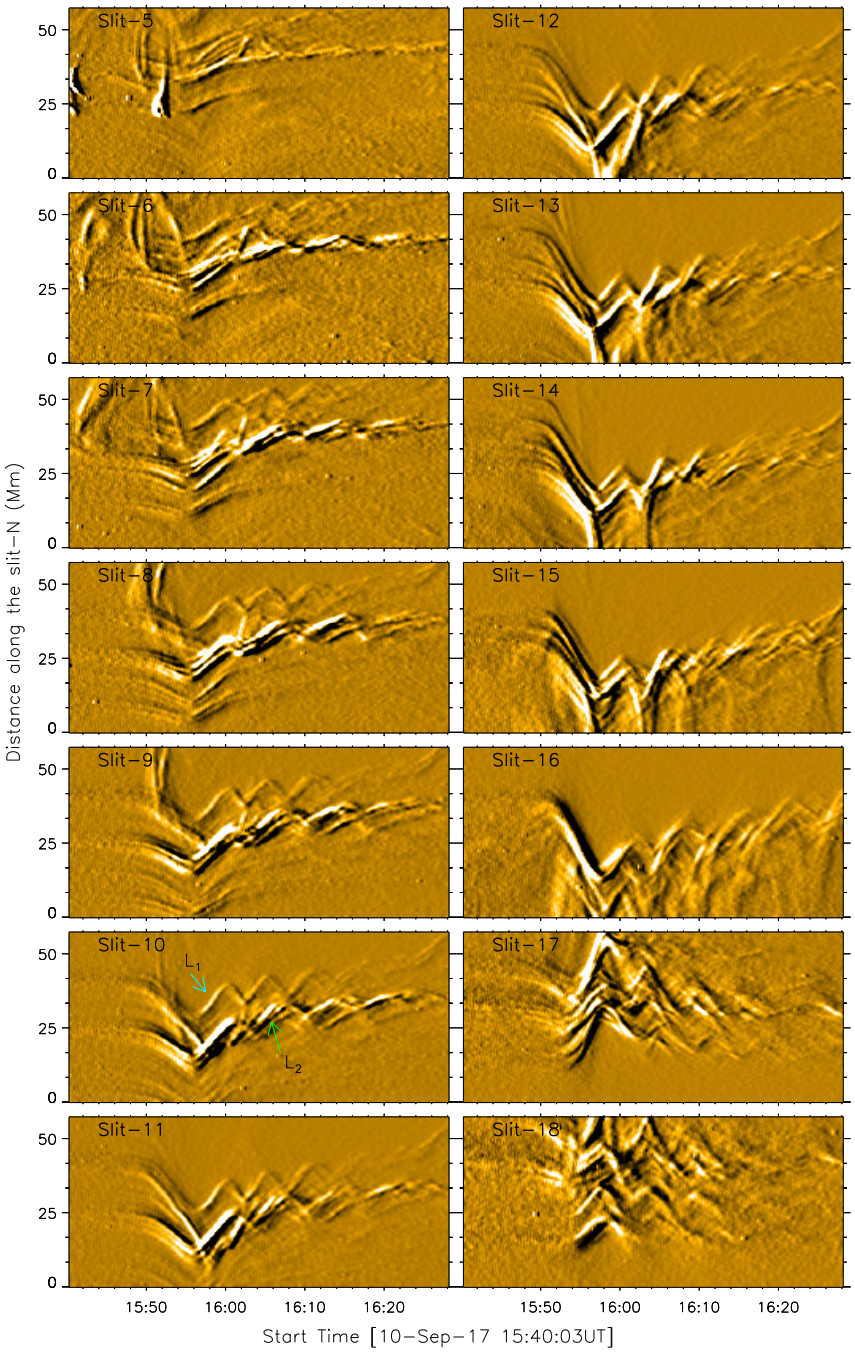

Figure 10. Space-time maps of AIA 171 Å intensity along 10 different slit positions (slit-5 to slit-18) across the L_1 and L_2 loops as shown in Figure 9. The cyan and green arrow marks the position of the loops, L_1 and L_2 in the space-time maps for the slit-10.

where, A is the amplitude, τ is the damping time, P is the period of oscillation and ϕ is the phase. We find that the damp fit does not precisely fit the loop positions. Therefore, to estimate more accurate the oscillation period, we compute the Fourier power spectra of the loop oscillation time-series as shown in the bottom panel of the Figure 11. We repeated this calculations for the 9 slit positions (8 to 15 & 18) for both the loops L_1 and L_2. The oscillation parameters obtained from the fit and Fourier spectra are listed in the Table 1 and 2 for the loops L_1 and L_2, respectively.

We find that the loop L_1 oscillates with a significantly larger amplitude than the loop L_2 which is also evident from their power spectra as shown in the Figure 11(bottom row). The average period of oscillations of the loop L_1 is found to be 5.75 ± 0.47 minutes with

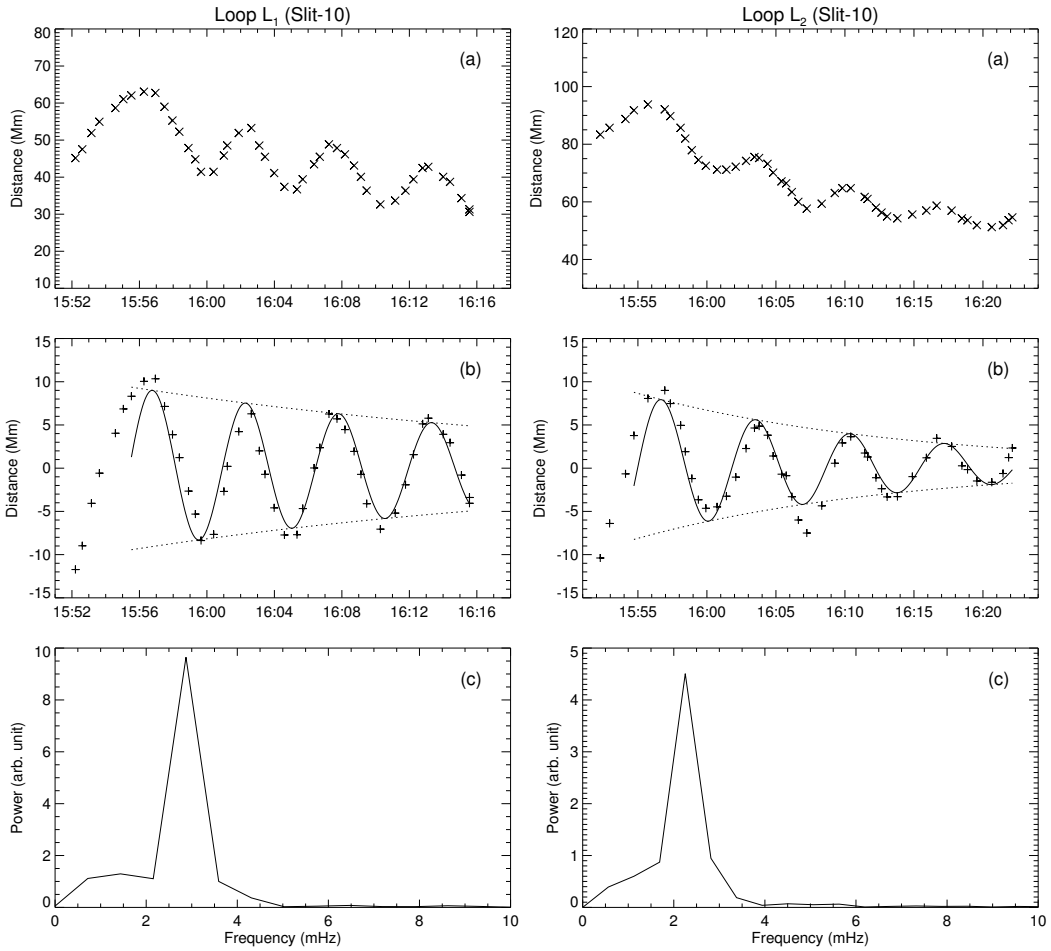

Figure 11. Transverse oscillations of coronal loops L_1 (left) and L_2 (right) across the slit-10. *(Top row)* The crosses correspond to the loop positions estimated from the space-time maps. *(Middle row)* Time series of the loop positions after subtracting a low degree polynomial. The solid curve represents the damp fit (Equation 1), *(Bottom row)* Fourier power spectra of the time series shown in the middle panel.

a damping time of $\tau = 30.78 \pm 11.54$ minutes while the average period of the loop L_2 is found to be $P = 7.20 \pm 0.31$ minutes with a damping time of $\tau = 16.00 \pm 5.90$ minutes. That is, the loop L_2 oscillates with a significantly larger period than the loop L_1 but with a shorter damping time and amplitude. The single peak in the power spectra of both the loops provides evidence that the oscillations are in fundamental mode.

Further to confirm the fundamental mode of oscillations in a coronal loop, we analysed the cross-spectra and the cross-phases in different times series obtained from different slits for the same loop (see Figure 12). The point of intersection between a line from the peak of cross-spectrum and curve of the phase-spectrum is taken as the phase difference of two points along the loop. The phase differences along the loop between slits determine whether the oscillations are in-phase. We did not find significant phase difference in slit positions of a loop. This confirmed that both the loops are oscillating in fundamental modes. However, these loops were found to be oscillating in different phases. The phase difference between the two loop was found to be around 33°.

We estimated the kink speed, Alfvén speed and the magnetic field by finding the loop length and the period of oscillations. The length of a coronal loop can be estimated more accurately by comparing their observations from two different viewpoints, *e.g.*, using one observation from an Extreme Ultraviolet Imager (EUVI)/Solar Terrestrial Relations Observatory (STEREO) and the other from SDO/AIA or both from STEREO A & B. This method gives more accurate length of the loop instead of a projected image on the plane of site. But, for this event, the oscillating loops are only seen in SDO/AIA observations and not in the STEREO/EUVI channels. Therefore, we cannot estimate the 3D loop geometry by the above said approach. We manually marked red cross points along the selected loop as

Table 1. Oscillations parameters of the coronal loop L_1 along different slit directions.

S.N.	Slit No. N	Amplitude (Mm)	Period from damp-fit $P_1(minute)$	Damping time $\tau(minute)$	Peak frequency $f(mHz)$	Period from power spectra $P_2(minute)$
1	8	11.12	5.97	54.86	2.49	6.70
2	9	13.08	6.08	28.18	2.69	6.20
3	10	13.64	5.85	29.48	2.69	6.20
4	11	11.18	5.55	30.41	2.87	5.80
5	12	11.82	5.12	14.58	3.09	5.40
6	13	11.14	5.30	21.67	3.09	5.40
7	14	9.64	5.16	37.84	3.12	5.33
8	15	12.70	5.55	19.70	3.14	5.30
9	18	3.56	6.17	40.34	3.06	5.44
		10.88±2.83	5.64±0.37	30.78±11.54	2.92±0.22	5.75±0.47

Table 2. Oscillation parameters of the loop L_2 along different slit directions.

S.N.	Slit No. N	Amplitude (Mm)	Period from damp-fit $P_1(minute)$	Damping time $\tau(minute)$	Peak frequency $f(mHz)$	Period from power spectra $P_2(minute)$
1	8	6.30	7.47	17.98	2.42	6.90
2	9	7.10	7.50	18.02	2.40	7.00
3	10	10.12	7.33	26.87	2.41	7.00
4	11	12.02	7.36	12.18	2.28	7.30
5	12	16.44	7.20	9.00	2.28	7.30
6	13	14.84	7.40	11.87	2.45	6.80
7	14	16.32	7.55	7.61	2.38	7.00
8	15	13.81	7.44	18.82	2.45	6.80
9	18	5.24	9.42	21.40	1.92	8.70
		11.35±4.10	7.63±0.64	16.00±5.90	2.33±0.16	7.20±0.31

shown in Figure 9 and an approximate loop length is determined by numerical integration. The errors on the loop length measurement is mainly due to the projection effect. Thus the estimated lengths of the coronal loops are listed in the Table 3. Previous studied showed that period of oscillations are proportional to the length of a loop (*e.g.*, Goddard and Nakariakov, 2016). But, we find that the smaller loop L_2 oscillates with a more extended period than the loop L_1. This could be due to error in the measurements of loop lengths.

For a fundamental mode of oscillation, the longitudinal phase speed can be expressed in terms of the period of kink oscillation (P) and the loop length (Roberts, Edwin, and Benz, 1984; Verwichte *et al.*, 2009),

$$V_{\rm ph} = \frac{2L}{P}. \tag{2}$$

Further, from the MHD wave theory, the fast kink standing waves are strongly dispersive with real wave number k and frequency ω. The phase speed of a fast kink mode, in the long wavelength ($k \ll 1$) and zero plasma -β limit, equals to the kink speed C_k (Edwin and Roberts, 1983). In the thin tube approximation of kink mode oscillations, C_k can also be represented (Roberts, Edwin, and Benz, 1984) as,

$$C_k = V_{A0}\sqrt{\frac{2}{1+\rho_{\rm ex}/\rho_{\rm in}}}, \tag{3}$$

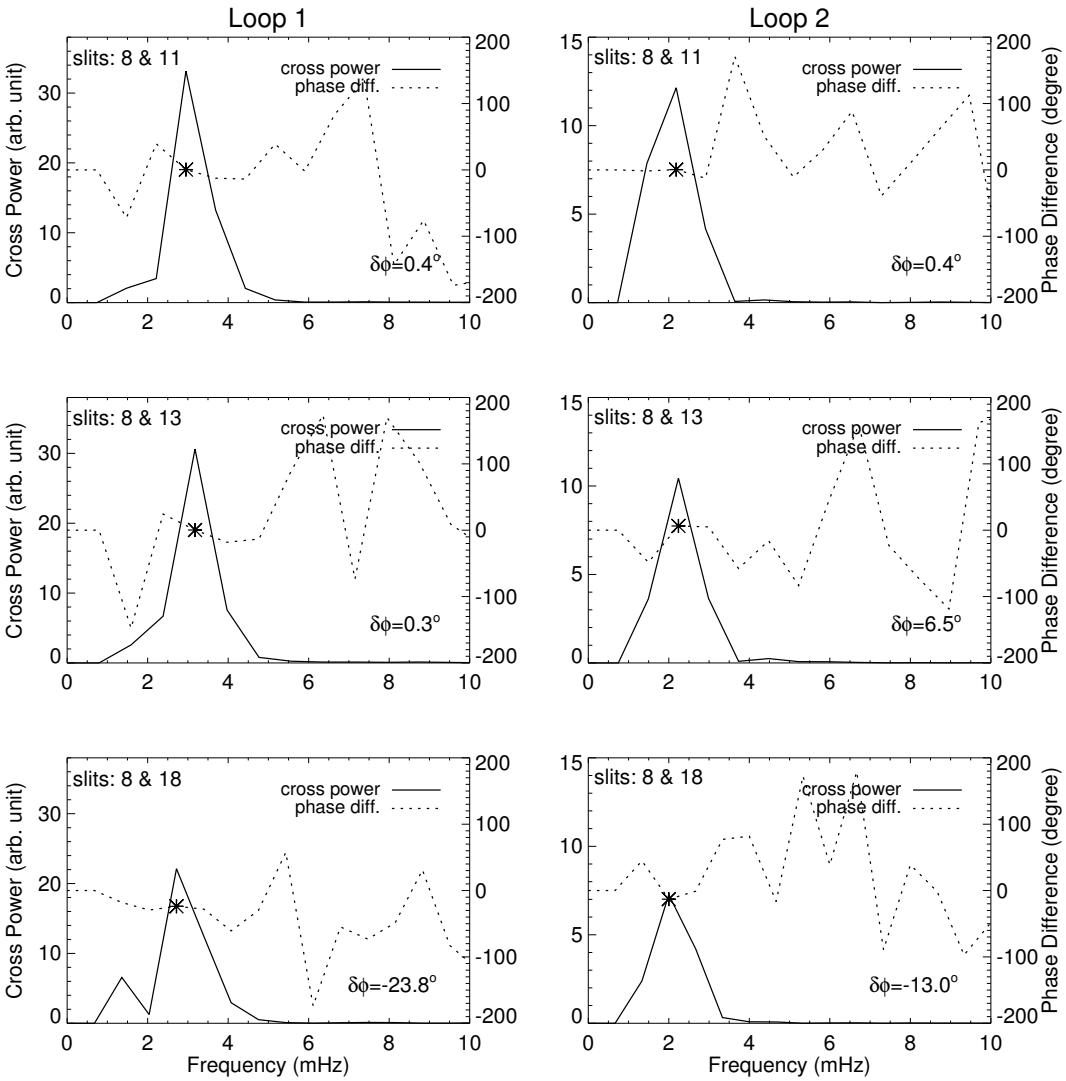

Figure 12. Cross-power spectra (solid curve) and the phase difference (dotted curve) profiles obtained from times series of the loop oscillations across the slits 8 & 11 (top row), 8 & 13 (middle row) and 8 & 18 (bottom row) for the coronal loops L_1 (left column) and L_2 (right column). For slits' positions, see Figure 9. The asterisks symbol '*' on the phase-profile marks the phase difference ($\delta\phi$) between two time series.

which is related with the internal Alfvén speed V_{A0} and the internal ($\rho_{\rm in}$) and external ($\rho_{\rm ex}$) plasma densities of the loop. The Alfvén speed is defined in terms of magnetic field and the density of the loop. Considering uniform magnetic field and the Equation 3, kink speed can be written as,

$$C_{\rm k} = B\sqrt{\frac{2}{\mu_0(\rho_{\rm in}+\rho_{\rm ex})}}, \tag{4}$$

where, B is the magnetic field strength in the loop and μ_0 is the permeability of free space. Assuming that the density ratio $\rho_{ex}/\rho_{in} \approx 0.1$ (Nakariakov *et al.*, 1999), the Alfvén speed ranges between,

$$\frac{2L}{\sqrt{2}P} \leq V_{A0} \leq \frac{2L}{P}, \tag{5}$$

and hence the magnetic field in the coronal loop can be expressed as,

$$B = V_{A0}\sqrt{4\pi\mu_c m_p n_e}, \tag{6}$$

where, $\mu_c = 1.27$ is the mean molecular weight in the corona, m_p is the proton mass. The electron density n_e in the coronal plasma can be taken as $(7-10) \times 10^9\, cm^{-3}$ (Sun *et al.*, 2013). Then the range of magnetic field can be expressed (Verwichte *et al.*, 2009; White and Verwichte, 2012; Nakariakov and Ofman, 2001) as,

$$\frac{2L}{\sqrt{2}P}\sqrt{\mu_c m_p n_e} \leq B \leq \frac{2L}{P}\sqrt{\mu_c m_p n_e} \tag{7}$$

Using above equations, and the oscillation properties of coronal loops, we can estimate the Alfvén's speed and the magnetic field in the coronal loops. Thus, computed values for the two loops are listed in the Table 3. The order of magnetic fields in the coronal loops seems to reasonable.

Table 3. Oscillation parameters, the magnetic fields and the Alfvén's speed in the coronal loops

Loop	Period $P(minute)$	Length (Mm)	Kink speed (kms^{-1})	Alfvén speed (kms^{-1})	Magnetic field (G)
L_1	5.75±0.47	193	4052.32±335.33	3005.28±248.69	14.26±1.69
L_2	7.20±0.31	160	2680.60±191.17	1987.99±141.78	9.58±1.35

4. Summary and Conclusions

Using the EUV intensity observations of solar corona, we analysed the transverse oscillations in the coronal loops of an active region that was located at the west limb of the solar disc. The active region was found to be a complex areas with mixed magnetic polarities. One of the footpoints of coronal loops were found to be anchored in the active region center and the other in the near by diffused polarity regions.

The initiation of the loop oscillations is found to be triggered by a plamoid erruption that was followed by a pre-flare which initiated reconnection of field lines leading to a large X8.2 class flare. During the pre-flare, a flux rope was found to be rising slowly then expanded and finally undergoes acceleration phase. The magnetic field lines seem to be reconnected during its expansion phase and a flare brightening was observed. This flux rope is found to be associated with the formation of a plasmoid. During the ejection of the plasmoid, the coronal loop interacts with the nearby loops and initiated oscillation before the impulsive phase of the main flare. We analysed the oscillation properties in two distinct coronal loops and computed the coronal magnetic fields.

We found that the loops oscillated with average periods of 5.75 minutes and 7.20 minutes, with average damping times of 30.78 minutes and 16.00 minutes, respectively. In the Fourier power spectra of the loop oscillation, we found a single peak that depicts the oscillation to be in the fundamental mode. Further from the phase analysis between two successive slit directions along a single loop, we confirm that different parts of the loop oscillate in the same phase. But the two loops are found to be oscillating with a phase difference of $\sim 33^o$. This could be due to different triggering times for their oscillations. The length of loops measured as $L_1 = 193\,\mathrm{Mm}$ and $L_2 = 160\,\mathrm{Mm}$. Generally, the period of oscillation is proportional to the length of the oscillating loop (Aschwanden and Boerner, 2011). Here the contrast could be due to error in the length measurement mainly caused by projection effect. Using the period of oscillations and loop lengths, we estimated the kink speed, Alfvén speed and hence the magnetic field associated with the oscillating loops. Thus the estimated magnetic fields in the coronal loops are found to be $\sim 40\,G$ and $\sim 26\,G$, respectively.

We observed flare induced shock wave propagating across the solar disc with an average speed of $1290\,\mathrm{km\,s^{-1}}$ and an acceleration of about $1.2\,\mathrm{km\,s^{-2}}$. These waves cover the entire solar disc and also stroked with the upper atmospheric layers. Initially, they traveled towards the southern polar regions and reflected on the disc. Other researchers have also reported

earlier (Seaton and Darnel, 2018; Liu *et al.*, 2018) that it is the first observation of a truly global EUV wave with SDO/AIA observations. From the SOHO/LASCO CME catalog, we also found that the main flare is accompanied with a fast propagating halo CME. Gopalswamy *et al.* (2018) reported that this CME was the highest eruption in the SOHO era with ground level enhancement (GLE) and solar energetic particle (SEP) event. We found that the flare generated shocks and associated CME started during the impulsive phase of the main Flare.

There are three possible source of the perturbations that leads to the oscillations in the coronal loops: (1) rising plasmoid increases in size due to reduction of density and pushed the coronal loop field lines from their equilibrium positions, (2) One of the flux tube suppressed the other loops to perturbed maximum amplitude oscillations, and (3) shock wave generated at the time of plasmoid ejection. It would be interesting to analyse such events on the solar disc and compare the magnetic field obtained from other methods such as extrapolations.

Acknowledgments This work uses the observational data obtained from the SDO/AIA & HMI and SOHO/LASCO. SOHO is project of international collaboration between ESA and NASA. The integrated X-ray flux data were obtained from GOES operated by National Oceanic and Atmospheric Administration, USA. We thanks Durgesh Tripathi of IUCAA for his valuable comments and suggestions which helped us to improve the manuscript. R.A.M. thankfully acknowledges the support by the NITC/FRG-2019 under which this work was carried out.

References

Anfinogentov, S., Nisticò, G., Nakariakov, V.M.: 2013, Decay-less kink oscillations in coronal loops. *Astron. Astrophys.* **560**, A107. DOI.

Aschwanden, M.J., Boerner, P.: 2011, Solar coronal loop studies with the atmospheric imaging assembly. i. cross-sectional temperature structure. *Astrophys. J.* **732**(2), 81. DOI.

Aschwanden, M.J., Schrijver, C.J.: 2011, Coronal loop oscillations observed with atmospheric imaging assembly—kink mode with cross-sectional and density oscillations. *Astrophys. J.* **736**(2), 102. DOI.

Aschwanden, M.J., Fletcher, L., Schrijver, C.J., Alexander, D.: 1999, Coronal loop oscillations observed with the transition region and coronal explorer. *Astrophys. J.* **520**(2), 880. DOI.

Brueckner, G.E., Howard, R.A., Koomen, M.J., Korendyke, C.M., Michels, D.J., Moses, J.D., Socker, D.G., Dere, K.P., Lamy, P.L., Llebaria, A., Bout, M.V., Schwenn, R., Simnett, G.M., Bedford, D.K., Eyles, C.J.: 1995, The large angle spectroscopic coronagraph (LASCO). *Solar Phys.* **162**(1-2), 357. DOI.

Doorsselaere, T.V., Nakariakov, V.M., Verwichte, E.: 2007, Coronal loop seismology using multiple transverse loop oscillation harmonics. *Astron. Astrophys.* **473**(3), 959. DOI.

Edwin, P.M., Roberts, B.: 1983, Wave propagation in a magnetic cylinder. *Solar Phys.* **88**(1-2). DOI.

Goddard, C.R., Nakariakov, V.M.: 2016, Dependence of kink oscillation damping on the amplitude. *Astron. Astrophys.* **590**, L5. DOI.

Goddard, C.R., Nisticò, G., Nakariakov, V.M., Zimovets, I.V.: 2016, A statistical study of decaying kink oscillations detected using SDO/AIA. *Astron. Astrophys.* **585**, A137. DOI.

Gopalswamy, N., Yashiro, S., Mäkelä, P., Xie, H., Akiyama, S., Monstein, C.: 2018, Extreme kinematics of the 2017 september 10 solar eruption and the spectral characteristics of the associated energetic particles. *Astrophys. J.* **863**(2), L39. DOI.

Heyvaerts, J., Priest, E.R.: 1983, Coronal heating by phase-mixed shear Alfven waves. *Astron. Astrophys.* **117**, 220. ADS.

Hollweg, J.V., Yang, G.: 1988, Resonance absorption of compressible magnetohydrodynamic waves at thin "surfaces". *J. Geophys. Res.* **93**(A6), 5423. DOI.

Jain, R., Maurya, R.A., Hindman, B.W.: 2015, Fundamental-mode oscillations of two coronal loops within a solar magnetic arcade. *Astrophys. J.* **804**(1), L19. DOI.

Lemen, J.R., Title, A.M., Akin, D.J., Boerner, P.F., Chou, C., Drake, J.F., Duncan, D.W., Edwards, C.G., Friedlaender, F.M., Heyman, G.F., Hurlburt, N.E., Katz, N.L., Kushner, G.D., Levay, M., Lindgren, R.W., Mathur, D.P., McFeaters, E.L., Mitchell, S., Rehse, R.A., Schrijver, C.J., Springer, L.A., Stern, R.A., Tarbell, T.D., Wuelser, J.-P., Wolfson, C.J., Yanari, C., Bookbinder, J.A., Cheimets, P.N., Caldwell, D., Deluca, E.E., Gates, R., Golub, L., Park, S., Podgorski, W.A., Bush, R.I., Scherrer, P.H., Gummin, M.A., Smith, P., Auker, G., Jerram, P., Pool, P., Soufli, R., Windt, D.L., Beardsley, S., Clapp, M., Lang, J., Waltham, N.: 2011, The atmospheric imaging assembly (AIA) on the solar dynamics observatory (SDO). *Solar Phys.* **275**(1-2), 17. DOI.

Liu, W., Jin, M., Downs, C., Ofman, L., Cheung, M.C.M., Nitta, N.V.: 2018, A truly global extreme ultraviolet wave from the SOL2017-09-10 x8.2+ solar flare-coronal mass ejection. *Astrophys. J.* **864**(2), L24. DOI.

Mitra, P.K., Joshi, B.: 2019, Preflare processes, flux rope activation, large-scale eruption, and associated x-class flare from the active region NOAA 11875. *Astrophys. J.* **884**(1), 46. DOI.

Moortel, I.D., Brady, C.S.: 2007, Observation of higher harmonic coronal loop oscillations. *Astrophys. J.* **664**(2), 1210. DOI.

Nakariakov, V.M., Ofman, L.: 2001, Determination of the coronal magnetic field by coronal loop oscillations. *Astron. Astrophys.* **372**(3), L53. DOI.

Nakariakov, V.M., Verwichte, E.: 2005, Coronal waves and oscillations. *Liv. Rev. Solar Phys.* **2**. DOI.

Nakariakov, V.M., Ofman, L., DeLuca, E.E., Roberts, B., Davila, J.M.: 1999, TRACE observation of damped coronal loop oscillations: Implications for coronal heating. *Science* **285**(5429), 862. DOI.

Nakariakov, V.M., Anfinogentov, S.A., Antolin, P., Jain, R., Kolotkov, D.Y., Kupriyanova, E.G., Li, D., Magyar, N., Nisticò, G., Pascoe, D.J., Srivastava, A.K., Terradas, J., Vasheghani Farahani, S., Verth, G., Yuan, D., Zimovets, I.V.: 2021, Kink Oscillations of Coronal Loops. *Space Sci. Rev.* **217**(6), 73. DOI. ADS.

Nindos, A., Patsourakos, S., Vourlidas, A., Tagikas, C.: 2015, How common are hot magnetic flux ropes in the low solar corona? a statistical study of euv observations. *Astrophys. J.* **808**(2), 117. DOI.

Nisticò, G., Nakariakov, V.M., Verwichte, E.: 2013, Decaying and decayless transverse oscillations of a coronal loop. *Astron. Astrophys.* **552**, A57. DOI.

O'Dwyer, B., Del Zanna, G., Mason, H.E., Weber, M.A., Tripathi, D.: 2010, SDO/AIA response to coronal hole, quiet Sun, active region, and flare plasma. *Astron. Astrophys.* **521**, A21. DOI. ADS.

Pascoe, D.J., Hood, A.W., Moortel, I.D., Wright, A.N.: 2012, Spatial damping of propagating kink waves due to mode coupling. *Astron. Astrophys.* **539**, A37. DOI.

Roberts, B., Edwin, P.M., Benz, A.O.: 1984, On coronal oscillations. *Astrophys. J.* **279**, 857. DOI.

Russell, A.J.B., Simões, P.J.A., Fletcher, L.: 2015, A unified view of coronal loop contraction and oscillation in flares. *Astron. Astrophys.* **581**, A8. DOI.

Seaton, D.B., Darnel, J.M.: 2018, Observations of an eruptive solar flare in the extended EUV solar corona. *Astrophys. J.* **852**(1), L9. DOI.

Shibata, K.: 1996, New observational facts about solar flares from yohkoh studies — evidence of magnetic reconnection and a unified model of flares. *Adv. Spa. Res.* **17**(4-5), 9. DOI.

Sun, X., Hoeksema, J.T., Liu, Y., Aulanier, G., Su, Y., Hannah, I.G., Hock, R.A.: 2013, Hot spline loops and the nature of a late-phase solar flare. *Astrophys. J.* **778**(2), 139. DOI.

Verwichte, E., Aschwanden, M.J., Doorsselaere, T.V., Foullon, C., Nakariakov, V.M.: 2009, Seismology of a large solar coronal loop from euvi/stereo observations of its transverse oscillation. *Astrophys. J.* **698**(1), 397. DOI.

White, R.S., Verwichte, E.: 2012, Transverse coronal loop oscillations seen in unprecedented detail by AIA/SDO. *Astron. Astrophys.* **537**, A49. DOI.

White, R.S., Verwichte, E., Foullon, C.: 2013, Anti-phase siignature of flare generated transverse loop oscillations. *Astrophys. J.* **774**(2), 104. DOI.

Yokoyama, T., Akita, K., Morimoto, T., Inoue, K., Newmark, J.: 2001, Clear evidence of reconnection inflow of a solar flare. *Astrophys. J.* **546**(1), L69. DOI.

Zimovets, I.V., Nakariakov, V.M.: 2015, Excitation of kink oscillations of coronal loops: statistical study. *Astron. Astrophys.* **577**, A4. DOI.